THE JOURNAL OF PHYSICAL CHEMISTRY C

Article

pubs.acs.org/JPCC

Molecular Origin of Donor- and Acceptor-Rich Domain Formation in Bulk-Heterojunction Solar Cells with an Enhanced Charge Transport Efficiency

Guankui Long,[†,‡] Rui Shi,[§,¶,‡] Yecheng Zhou,[⊥] Ailin Li,[∥] Bin Kan,[†] Wei-Ru Wu,[▽,○] U-Ser Jeng,[▽,○] Tao Xu,[◆] Tianying Yan,[∥] Mingtao Zhang,[†] Xuan Yang,[†] Xin Ke,[†] Litao Sun,[◆] Angus Gray-Weale,[⊥] Xiangjian Wan,[†] Hongtao Zhang,[†] Chenxi Li,[†] Yanting Wang,[*,§,#] and Yongsheng Chen[*,†]

[†]State Key Laboratory and Institute of Elemento-Organic Chemistry, Collaborative Innovation Center of Chemical Science and Engineering, School of Materials Science and Engineering, Nankai University, Tianjin 300071, China

[§]CAS Key Laboratory of Theoretical Physics, Institute of Theoretical Physics, Chinese Academy of Sciences, 55 East Zhongguancun Road, P.O. Box 2735, Beijing 100190, China

[¶]Department of Fundamental Engineering, Institute of Industrial Science, University of Tokyo, 4-6-1 Komaba, Meguro-ku, Tokyo 153-8505, Japan

[∥]Institute of New Energy Material Chemistry, Tianjin Key Laboratory of Metal- and Molecule-Based Material Chemistry, Collaborative Innovation Center of Chemical Science and Engineering (Tianjin), School of Materials Science and Engineering, Nankai University, Tianjin 300071, China

[⊥]School of Chemistry, University of Melbourne, Parkville, VIC 3010, Australia

[#]School of Physical Sciences, University of Chinese Academy of Sciences, 19A Yuquan Road, Beijing 100049, China

[▽]National Synchrotron Radiation Research Center, Hsinchu Science Park, Hsinchu 30077, Taiwan

[○]Chemical Engineering Department, National Tsing-Hua University, Hsinchu 30013, Taiwan

[◆]SEU-FEI Nano-Pico Center, Key Laboratory of MEMS of Ministry of Education, Southeast University, Nanjing 210096, China

Supporting Information

ABSTRACT: Understanding the origin of different morphologies in bulk-heterojunction solar cells can provide effective guidelines to rational control of the morphologies in the active layer. Here, we have uncovered the importance of molecular interactions on the morphologies for not only donor materials but also for fullerene acceptors in organic solar cells through the multiscale coarse-graining molecular dynamic simulations at the real device level (~83 nm × 83 nm × 83 nm). It is found that oligothiophene donors with polar end groups could not only facilitate the formation of continuous donor network but also promote the aggregation and connection of fullerenes toward efficient hole and electron transport. On the contrary, fullerenes are well dispersed at the molecule levels in the less polar oligothiophene matrix and thus contribute to the poor electron transport mobility and device performance, which is consistent with the observed differences in both morphology and charge transport properties of these two systems. These results would provide effective guidelines for the rational molecule design and morphology control to further enhance the device performance of organic solar cells.

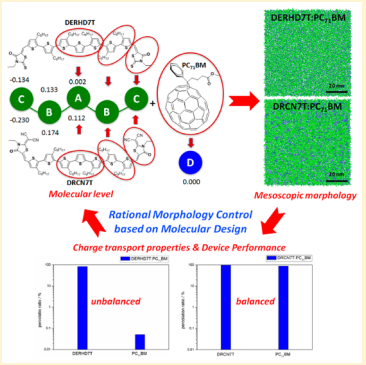

1. INTRODUCTION

Bulk-heterojunction organic solar cells (BHJ-OSCs) composed of electron-donating and electron-accepting materials have received much attention in the past 2 decades owing to their fascinating features, such as low cost, light weight, solution-processability, and high-mechanical flexibility.[1] Although the power conversion efficiency (PCE) for BHJ-OSCs has recently been significantly improved to over 11%,[2] it does not yet meet the requirement for commercialization. Besides the influence of interlayers[3,4] and novel device structures,[5,6] materials[7−12] and morphologies[13−15] in the active layer decisively control the performance of OSCs. Compared with the complex morphologies owning to the mixture nature of electron-donating and accepting materials and other additives,[16,17] some effective strategies have been successfully developed and employed to tune the optical and electronic properties of both donor and acceptor materials.[18−23] However, due to the lack of detailed understanding at the mesoscopic level, there still has been no efficient strategy to optimize and control the morphology in the active layer, and the only way to achieve optimized morphology

Received: November 23, 2016
Revised: February 20, 2017
Published: February 22, 2017

DOI: 10.1021/acs.jpcc.6b11824
J. Phys. Chem. C 2017, 121, 5864−5870

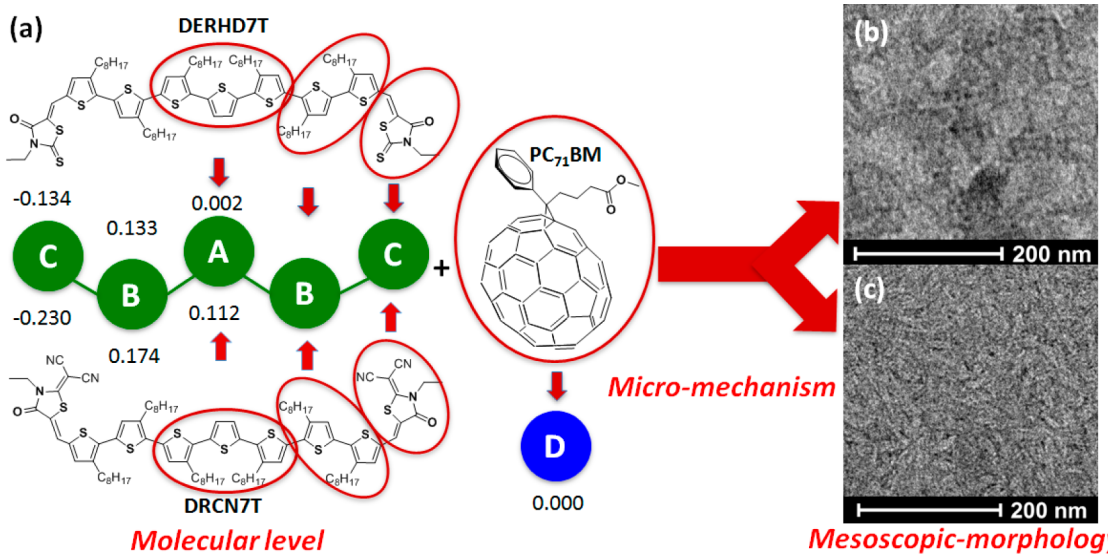

Figure 1. (a) Chemical structures of **DERHD7T**, **DRCN7T**, and $PC_{71}BM$, and the corresponding coarse-grained models with partial charges denoted for all coarse-grained sites. Bright-field TEM images of the blended **DERHD7T**:$PC_{71}BM$ (b) and **DRCN7T**:$PC_{71}BM$ (c) films are also shown for comparison.

in the device is still based on the iterative and time-consuming trial-and-error processes.[24−28] Therefore, understanding the relationship between molecular structures and morphologies is essential for further enhancing the performance of BHJ-OSCs through rational morphology control based on molecular design. Molecular dynamics (MD) simulations[29−37] were successfully employed to investigate the blended states of donors and acceptors in the active layer, and tremendous progresses were achieved.[38−42] However, most of the simulated boxes are even smaller than the experimental domain size, and the molecular origin of different morphologies is still unclear. Thus, the large-scale coarse-graining MD simulations[43−49] at the real device levels (∼100 nm) are extremely needed for systematically investigating the origin of different morphologies at the molecular level in OSCs.

In our previous studies, it has been found that two very similar donor molecules, **DERHD7T** and **DRCN7T** (the chemical structures are shown in Figure 1) behave very differently in their OSC devices with the same acceptor, $PC_{71}BM$, and **DRCN7T** performs much better than **DERHD7T** despite the fact that they have the same backbone structure and substituted groups except a small difference in their end groups.[50] Thus, it is vital to explore and understand why such a small difference in molecular structure could result in so large difference in photovoltaic performances. In this work, by combining MD simulation using the multiscale coarse-grained (MS-CG) model[51,52] at the real device scale (∼83 nm × 83 nm × 83 nm) with the experimental morphology results, it is found that fullerenes are well dispersed at the molecular level in the less polar matrix of **DERHD7T**, but aggregate strongly in the more polar **DRCN7T**:$PC_{71}BM$ system, and thus lead to better and continuous hole and electron-transport channels in the latter system. As a result, the percolation ratio[45] for fullerene phases to the electrodes increases drastically from 0.05% for **DERHD7T**:$PC_{71}BM$ to 90% for **DRCN7T**:$PC_{71}BM$ systems, respectively, consistent with the experimental morphologies and mobility observations. Our results reveal the important influence of molecular design on the device performance of BHJ-OSCs, by tuning the morphologies of not only donor materials but also fullerene acceptors.

2. COMPUTATIONAL DETAILS

The CG MD simulations were carried out with the DL_POLY program (version 2.14).[53] The details of the MS-CG models are given in the Supporting Information. The size of the simulation box with the periodic boundary condition (PBC) applied is ca. 83 nm × 83 nm × 83 nm, which is closed to the thickness of the active layer (∼100 nm) in real OSC devices. We note that a large-scale simulation is crucial for this work, because of the formation of large domains in the system.[50] A small simulation box may lead to serious finite size effect (see Figure S1 for more details).

As shown in Figure 1, the fullerene acceptor is coarse-grained as CG site **D**, the central trithiophene units in oligothiophene donors as CG sites **A**, the bridged dithiophene units as CG sites **B**, and end groups as CG sites **C**. The partial charge of each CG site, denoted in Figure 1, is the sum of the partial charges of all underlying atoms, and the force-field parameters for the bonded interactions at the CG level, listed in Tables S2 and S3, have been obtained by fitting the numerical curves provided by the MS-CG program with appropriate functions.[51,52]

3. RESULTS AND DISCUSSION

3.1. The Experimental Morphologies. Although the two donor molecules are very similar, their slight difference in the small end groups has a significant influence on the mesoscopic morphologies of their mixtures with $PC_{71}BM$. As shown by the bright field transmission electron microscopy (BF-TEM) images in Figure 1, parts b and c, the fullerene acceptors are well dispersed in the **DERHD7T**-rich matrix, while a bicontinuous interpenetrating network with well-expressed fibrillar structures were spread out through the **DRCN7T**:$PC_{71}BM$ film. By replacing the thio groups with the stronger electron-withdrawing dicyanomethylene (DCM) groups, **DRCN7T** was expected to have an enhanced polarity and intermolecular interaction than that of **DERHD7T**, which was confirmed by the density functional theory (DFT)

DOI: 10.1021/acs.jpcc.6b11824
J. Phys. Chem. C 2017, 121, 5864−5870

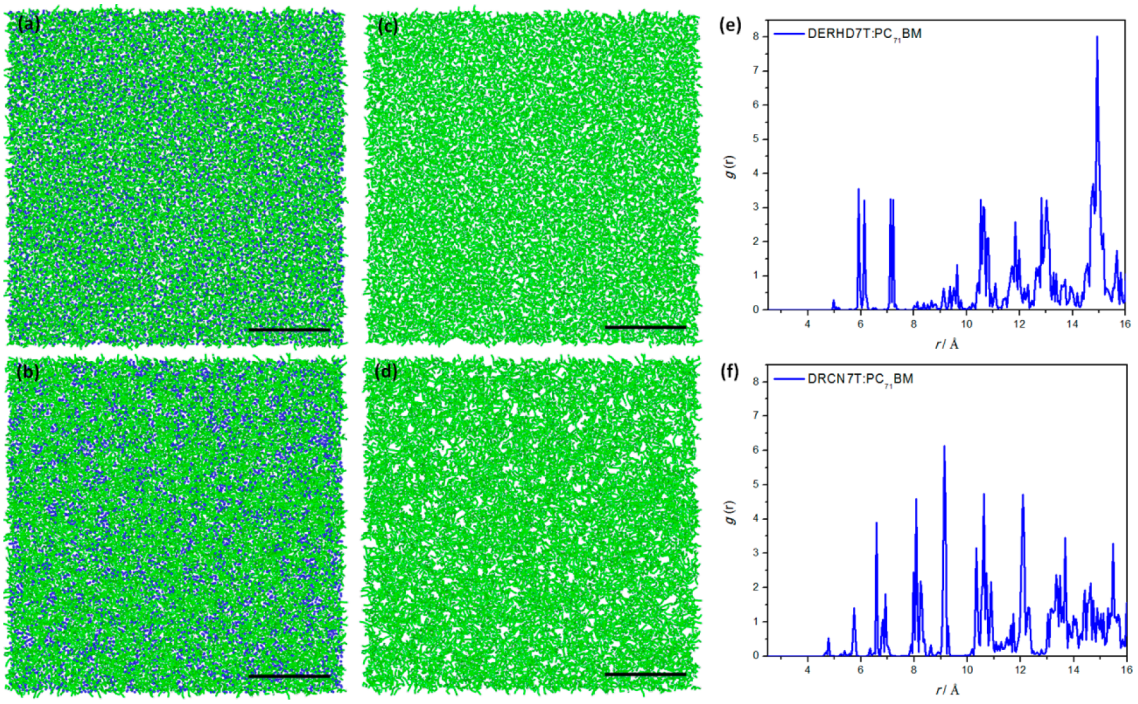

Figure 2. Sliced snapshot of the simulated morphologies (83 nm ×83 nm ×4 nm) for the **DERHD7T**:$PC_{71}BM$ (a) and **DRCN7T**:$PC_{71}BM$ (b) blended films. The oligothiophene-donor-only snapshot for **DERHD7T**:$PC_{71}BM$ (c) and **DRCN7T**:$PC_{71}BM$ (d) blended films are also shown for comparison. The oligothiophene chains were colored with green and fullerenes were colored with blue. The scale bars are 20 nm in parts a–d. The RDFs for the central trithiophene units of the oligothiophene donors (CG site **A**) in the **DERHD7T**:$PC_{71}BM$ (e) and **DRCN7T**:$PC_{71}BM$ (f) blends are also plotted.

calculations[54] at the *w*B97XD/6-31G* level, demonstrating that the binding energy increases significantly from 75.28 kcal/mol for **DERHD7T** π-dimers to 78.75 kcal/mol for **DRCN7T** π-dimers (Figure S2). With this, the MD simulations with the MS-CG models were then performed to investigate the micromechanism governing the formation of mesoscopic morphology due to molecular interactions.

3.2. The Simulated Morphologies from Coarse-Graining Molecular Dynamic Simulations. The snapshots of 4 nm-thick slices (83 nm ×83 nm in the other two dimensions) for the two investigated systems have been cut out from the simulated PBC box and are shown in Figure 2. It can be seen that fullerene acceptors are well dispersed at the molecular level in the less polar **DERHD7T** matrix (Figure 2 parts a and c), while the **DRCN7T** molecules form continuous networks (Figure 2, parts b and d) with strong fullerene aggregations, which are in generally consistent with the BF-TEM results shown in Figure 1. The resulting continuous charge transport channels for both holes and electrons in the **DRCN7T**:$PC_{71}BM$ blend would greatly influence the charge transport properties, as discussed below.

The heterogeneity order parameter (HOP),[55] which was successfully developed to investigate the degree of aggregations in ionic liquids with high reliability in our previous studies,[56] was employed to study the degrees of aggregation of different CG sites in the above two systems. A larger HOP value corresponds to a higher degree of aggregation (see the Supporting Information for more details),[55] and details of HOP are described in the Supporting Information. As shown in Table S4, the HOPs for the center-of-masses (COMs) of $PC_{71}BM$ (sites **D**) are 17.88 and 15.92 in the **DRCN7T**:$PC_{71}BM$ and **DERHD7T**:$PC_{71}BM$ blends, respectively. The larger HOP for fullerenes in the **DRCN7T**:$PC_{71}BM$ system indicates that fullerenes pack more tightly than that in **DERHD7T**:$PC_{71}BM$. Consistently, the COMs of the end groups (sites **C**) in **DRCN7T**:$PC_{71}BM$ also have a larger HOP value of 16.88 than that of 16.17 for **DERHD7T**:$PC_{71}BM$, demonstrating stronger polar attractions between the end groups of **DRCN7T** molecules, partly attributed to the significantly increased partial charges of the end groups from −0.134*e* for **DERHD7T** to −0.230*e* for **DRCN7T**, respectively (as shown in Figure 1).

3.3. The Mesoscopic Intermolecular Structure of Oligothiophene Donors and Evidence from the Wide-Angle X-ray Diffractions. The mesoscopic intermolecular structures of both oligothiophene donors and fullerene acceptors were then systematically quantified by the COM radial distribution function (RDF). As shown in Figure 2, parts e and f, both **DRCN7T**:$PC_{71}BM$ and **DERHD7T**:$PC_{71}BM$ systems exhibit very sharp and regular RDF peaks between the COMs of the central trithiophene units (sites **A**), indicating that the oligothiophene donors in both systems exhibit very strong crystalline-like behaviors, consistent with the experimentally observed (100), (200), (300), and (010) diffraction peaks in both systems through two-dimensional-grazing incidence wide-angle X-ray diffractions (2D-GIWAXD).[50] On the other hand, the COM RDFs for the end groups (sites **C**), shown in Figure S3, exhibit much stronger RDF peaks for **DRCN7T**:$PC_{71}BM$ than **DERHD7T**:$PC_{71}BM$, which further manifests the existence of stronger intermolecular interactions between **DRCN7T** molecules owning to the polar end groups. This also agrees well with the experimental results that the (001) diffraction peak (the orientation along the backbone directions of oligothiophenes) only observed through 2D-GIWAXD in the **DRCN7T**:$PC_{71}BM$ blends.[50,57] Thus, in the blends with the fullerene acceptor, the relatively stronger

DOI: 10.1021/acs.jpcc.6b11824
J. Phys. Chem. C 2017, 121, 5864−5870

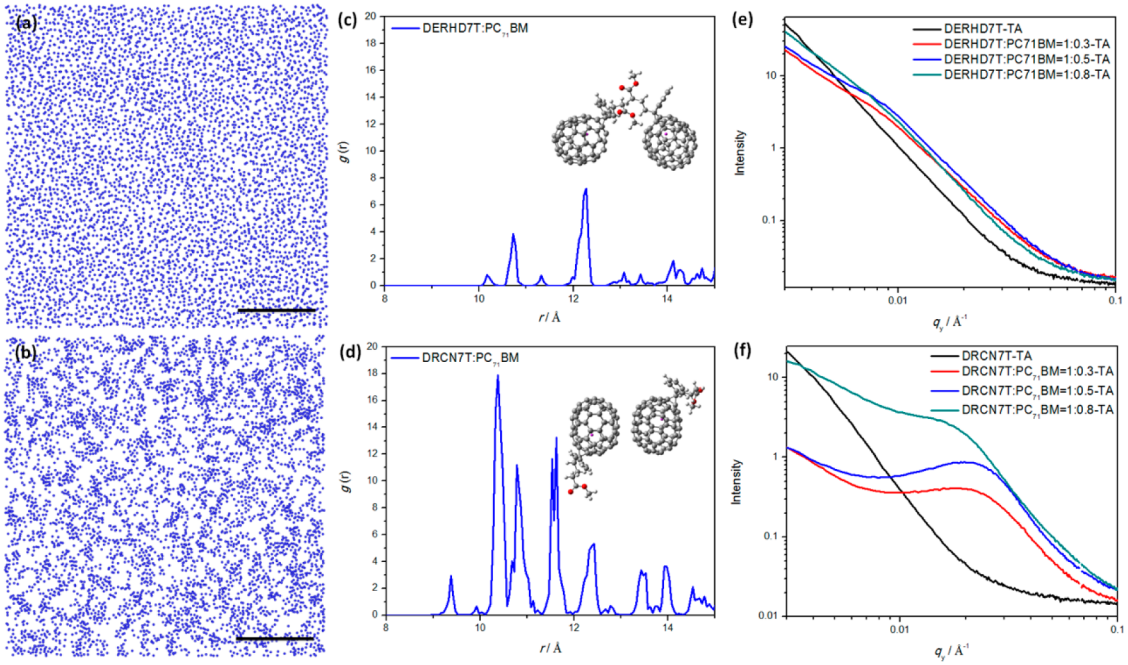

Figure 3. Sliced simulation snapshots with fullerene acceptors only (~83 nm × 83 nm × 4 nm) for **DERHD7T**:$PC_{71}BM$ (a) and **DRCN7T**:$PC_{71}BM$ (b). The scale bars are 20 nm. The RDFs for the fullerene acceptors in the **DERHD7T**:$PC_{71}BM$ (c) and **DRCN7T**:$PC_{71}BM$ (d) blends and the in-plane GISAXS profiles of the **DERHD7T**:$PC_{71}BM$ (e) and **DRCN7T**:$PC_{71}BM$ (f) blend films with different weight ratios (1:0, 1:0.3, 1:0.5 and 1:0.8) are also plotted for comparison.

polarity of **DRCN7T** molecules than **DERHD7T** encourages nonpolar fullerene molecules to aggregate, as analyzed in details below.

3.4. The Mesoscopic Intermolecular Structure of Fullerene Acceptors and Evidence from Small-Angle X-ray Scattering. Since **DRCN7T** molecules are more polar than **DERHD7T**, nonpolar $PC_{71}BM$ molecules should have a stronger degree of aggregation in the former blend than the latter.[58] The difference in fullerene spatial distributions in the two systems is better illustrated by only displaying fullerene molecules in the above sliced simulation snapshots (Figure 3, parts a and b). The COM RDFs for the fullerenes in these two systems have also been calculated and shown in Figure 3, parts c and d. The lower fullerene RDF peaks in **DERHD7T**:$PC_{71}BM$ (Figure 3c) confirms that fullerenes pack loosely in the blend with **DERHD7T**. By contrast, five distinctive high RDF peaks ranging from 9 to 13 Å are observed in the **DRCN7T**:$PC_{71}BM$ blend (Figure 3d), indicating the existence of highly ordered structures of fullerenes (Figure 3b). To experimentally confirm the two different behaviors of fullerenes in these two systems, the two-dimensional-grazing incidence small-angle X-ray scattering (2D-GISAXS) was performed on both pure oligothiophene donor films and their BHJ blends with $PC_{71}BM$ (Figure 3, parts e and f). A series of **DERHD7T**:$PC_{71}BM$ and **DRCN7T**:$PC_{71}BM$ samples with different weight ratios varying from 1:0, 1:0.3, 1:0.5 to 1:0.8 were measured under the same conditions. As shown in Figure 3f, the scattering peak for **DRCN7T**:$PC_{71}BM$ samples is gradually enhanced with increasing $PC_{71}BM$ content. Thus, the broad peak at q of 0.007−0.04 $Å^{-1}$ in the **DRCN7T**:$PC_{71}BM$ blend is ascribed to the scattering of aggregated fullerene domains, as reported in literature.[59] By contrast, the 2D-GISAXS pattern for the **DERHD7T**:$PC_{71}BM$ film does not show any obvious peak and almost retains the same with increasing $PC_{71}BM$ content (Figure 3e), which manifests that fullerene molecules do not aggregate in the **DERHD7T**:$PC_{71}BM$ blend.

In order to obtain the theoretical fullerene domain size, we have calculated the structure factors ($S(q)$) of fullerenes (site **D**). As shown in Figure S4, the structure factors of fullerenes in both **DRCN7T**:$PC_{71}BM$ and **DERHD7T**:$PC_{71}BM$ blends match well with the experimental PXRD of pure $PC_{71}BM$ with q > 0.5 $Å^{-1}$, which further confirm the reliability of our CG-MD models and simulation procedures. The $S(q)$ of fullerenes in **DRCN7T**:$PC_{71}BM$ and **DERHD7T**:$PC_{71}BM$ systems exhibit peaks at 0.68 and 0.44 $Å^{-1}$, corresponding to intermolecular distances of 9.2 and 14.1 Å, respectively. This indicates that fullerenes are closely packed in **DRCN7T**:$PC_{71}BM$, while loosely packed with larger intermolecular distance in **DERHD7T**:$PC_{71}BM$. This is also consistent with the different behaviors of RDFs and snapshots of fullerenes in the two blends as discussed above. On the other hand, only the fullerenes in **DRCN7T**:$PC_{71}BM$ exhibit the domain size $S(q)$ peak at ~0.08 $Å^{-1}$ (as shown in Figure S4), and thus, the theoretical domain spacing of fullerene aggregates in **DRCN7T**:$PC_{71}BM$ is 7.85 nm, which agrees well with the actual fullerene domain size of 6.88 ± 0.51 nm deduced from 2D-GISAXS.[35]

3.5. Correlation of the Percolation Ratios of Oligothiophene or Fullerene Phases to Electrodes with Experimental Charge Transport Mobilities and Device Performances. The variation of the morphologies significantly influence the charge transport properties and thus the device performances,[16,17] so the percolation ratios for both oligothiophene and fullerene phases to the electrodes[45] were calculated to quantify the hole and electron transport properties in the above two different morphologies. Considering that isolated oligothiophene donor (or fullerene) domains can act as the recombination center obstructing the transportation of holes and electrons toward the respected electrodes, a higher

DOI: 10.1021/acs.jpcc.6b11824
J. Phys. Chem. C 2017, 121, 5864−5870

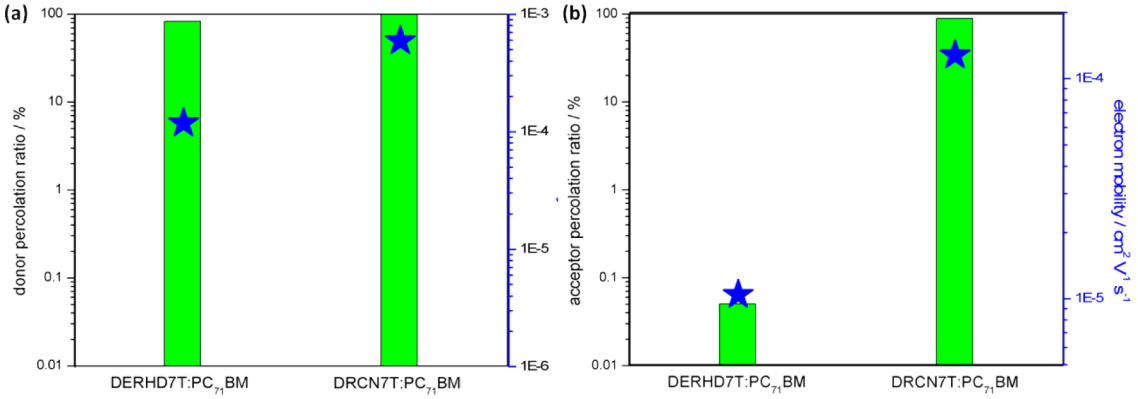

Figure 4. (a) Percolation ratios of oligothiophene molecules in the **DERHD7T**:$PC_{71}BM$ and **DRCN7T**:$PC_{71}BM$ systems. (b) Percolation ratios of $PC_{71}BM$ molecules in the **DERHD7T**:$PC_{71}BM$ and **DRCN7T**:$PC_{71}BM$ systems. The experimental hole and electron mobilities in both BHJ blends are also shown for comparison.

percolation ratio could ensure an expedient charge transport channel and thus better photovoltaic performances.[60] Details of the percolation-ratio calculations can be found in the Supporting Information. Unlike fullerene acceptors, the calculations of the percolation ratios for oligothiophene donors are not straightforward since each molecule has five CG sites. We have overcome this difficulty by regarding two oligothiophene molecules as connected if the intermolecular distance between any of their two sites is within the cutoff value of 6.0 Å (refer to the Supporting Information). As shown in Figure 4a, for the donor molecules, the **DRCN7T**:$PC_{71}BM$ system has a larger percolation ratio (99%) than that of **DERHD7T**:$PC_{71}BM$ (83%), coincident with the experimental observed enhancement of hole transport mobilities from 1.18×10^{-4} cm^2 V^{-1} $s^{-1}$for **DERHD7T**:$PC_{71}BM$ blends to 5.91×10^{-4} cm^2 V^{-1} s^{-1} for **DRCN7T**:$PC_{71}BM$ systems, respectively.[50] The percolation ratios for fullerenes are dramatically different, which are 90% for the **DRCN7T**:$PC_{71}BM$ system and only 0.05% for the **DERHD7T**:$PC_{71}BM$ blend by using a cutoff distance of 13 Å (refer to the Supporting Information). This is also consistent with the experimentally observed dramatic increase of electron mobility from 1.04×10^{-5} for **DERHD7T**:$PC_{71}BM$ to 1.28×10^{-4} cm^2 V^{-1} s^{-1} for **DRCN7T**:$PC_{71}BM$ blends, respectively.[50] Thus, the unbalanced hole and electron percolations in the **DERHD7T**:$PC_{71}BM$ system should account for the lower fill factor (FF) of 0.52 and poorer PCE of 4.35%, while the **DRCN7T**:$PC_{71}BM$ system has an enhanced FF of 0.69 and PCE of 9.30% owing to its balanced hole and electron percolations.[50]

4. CONCLUSION

The multiscale coarse-graining molecular dynamics simulations at the real device scale (~83 nm × 83 nm × 83 nm) were employed to systematically investigate the influence of donor intermolecular interactions on the mesoscopic morphologies of BHJ-OSCs, and consistent results with experiments are obtained. It is found that polar electron-donating molecules could facilitate the aggregation and connection of both donors and nonpolar acceptors, resulting in efficient hole and electron transport. By contrast, in less polar donor systems, fullerenes are dispersed due to the relatively weaker donor−donor intermolecular interaction, thus leading to poor electron transport mobility and device performance. Our results indicate that mesoscopic morphologies in the active layer can be directly predicted from molecular structures by employing the multiscale coarse-graining molecular dynamics simulation methodology, which provides a more efficient alternative method other than the time-consuming experimental try-and-error approach employed currently and thus facilitates the rational molecular design and morphology optimization toward enhanced device performances.

■ ASSOCIATED CONTENT

Supporting Information

The Supporting Information is available free of charge on the ACS Publications website at DOI: 10.1021/acs.jpcc.6b11824.

Details of simulations and experimental results (PDF)

■ AUTHOR INFORMATION

Corresponding Authors

*E-mail: (Y.W.) wangyt@itp.ac.cn.
*E-mail: (Y.C.) yschen99@nankai.edu.cn.

ORCID

Guankui Long: 0000-0002-1826-3736
Yecheng Zhou: 0000-0001-8222-7193
U-Ser Jeng: 0000-0002-2247-5061
Yongsheng Chen: 0000-0003-1448-8177

Author Contributions

‡These authors contributed equally to this work.

Notes

The authors declare no competing financial interest.

■ ACKNOWLEDGMENTS

The authors gratefully acknowledge financial support from the MOST (Grants 2014CB643502, 2013CB932804, and 2012CB933401), NSFC (Grants 91433101, 51422304, 51373078, 11274319, and 11421063), NSF of Tianjin City (Grant 13RCGFGX01121) and PCSIRT (IRT1257). We thank Dr. Dongchuang Wu and Dr. Zhou Xu at FEI Company for providing the TEM measurements and the 23A SWAXS Endstation of the National Synchrotron Radiation Research Center in Taiwan for providing beam time. The MS-CG MD simulations were performed on the HPC Cluster of ITP-CAS in Beijing and TianHe-1(A) at the National Supercomputer Center in Tianjin, China.

DOI: 10.1021/acs.jpcc.6b11824
J. Phys. Chem. C 2017, 121, 5864−5870

REFERENCES

(1) Beaujuge, P. M.; Fréchet, J. M. J. Molecular Design and Ordering Effects in π-Functional Materials for Transistor and Solar Cell Applications. *J. Am. Chem. Soc.* **2011**, *133*, 20009−20029.

(2) Zhao, J.; Li, Y.; Yang, G.; Jiang, K.; Lin, H.; Ade, H.; Ma, W.; Yan, H. Efficient Organic Solar Cells Processed from Hydrocarbon Solvents. *Nat. Energy* **2016**, *1*, 15027.

(3) Zhou, Y.; Fuentes-Hernandez, C.; Shim, J.; Meyer, J.; Giordano, A. J.; Li, H.; Winget, P.; Papadopoulos, T.; Cheun, H.; Kim, J.; et al. A Universal Method to Produce Low-Work Function Electrodes for Organic Electronics. *Science* **2012**, *336*, 327−332.

(4) Li, C. Z.; Chang, C. Y.; Zang, Y.; Ju, H. X.; Chueh, C. C.; Liang, P. W.; Cho, N.; Ginger, D. S.; Jen, A. K. Y. Suppressed Charge Recombination in Inverted Organic Photovoltaics via Enhanced Charge Extraction by Using a Conductive Fullerene Electron Transport Layer. *Adv. Mater.* **2014**, *26*, 6262−6267.

(5) Li, G.; Chu, C.; Shrotriya, V.; Huang, J.; Yang, Y. Efficient inverted polymer solar cells. *Appl. Phys. Lett.* **2006**, *88*, 253503.

(6) He, Z.; Zhong, C.; Su, S.; Xu, M.; Wu, H.; Cao, Y. Enhanced power-conversion efficiency in polymer solar cells using an inverted device structure. *Nat. Photonics* **2012**, *6*, 593−597.

(7) Cheng, Y. J.; Yang, S. H.; Hsu, C. S. Synthesis of Conjugated Polymers for Organic Solar Cell Applications. *Chem. Rev.* **2009**, *109*, 5868−5923.

(8) Zhou, H.; Yang, L.; You, W. Rational Design of High Performance Conjugated Polymers for Organic Solar Cells. *Macromolecules* **2012**, *45*, 607−632.

(9) Mishra, A.; Bäuerle, P. Small Molecule Organic Semiconductors on the Move: Promises for Future Solar Energy Technology. *Angew. Chem., Int. Ed.* **2012**, *51*, 2020−2067.

(10) Coughlin, J. E.; Henson, Z. B.; Welch, G. C.; Bazan, G. C. Design and Synthesis of Molecular Donors for Solution-Processed High-Efficiency Organic Solar Cells. *Acc. Chem. Res.* **2014**, *47*, 257−270.

(11) Walker, B.; Kim, C.; Nguyen, T. Q. Small Molecule Solution-Processed Bulk Heterojunction Solar Cells. *Chem. Mater.* **2011**, *23*, 470−482.

(12) Roncali, J.; Leriche, P.; Blanchard, P. Molecular Materials for Organic Photovoltaics: Small is Beautiful. *Adv. Mater.* **2014**, *26*, 3821−3838.

(13) Müller-Buschbaum, P. The Active Layer Morphology of Organic Solar Cells Probed with Grazing Incidence Scattering Techniques. *Adv. Mater.* **2014**, *26*, 7692−7709.

(14) Chen, W.; Nikiforov, M. P.; Darling, S. B. Morphology Characterization in Organic and Hybrid Solar Cells. *Energy Environ. Sci.* **2012**, *5*, 8045−8074.

(15) Rivnay, J.; Mannsfeld, S. C. B.; Miller, C. E.; Salleo, A.; Toney, M. F. Quantitative Determination of Organic Semiconductor Microstructure from the Molecular to Device Scale. *Chem. Rev.* **2012**, *112*, 5488−5519.

(16) Liu, F.; Gu, Y.; Shen, X.; Ferdous, S.; Wang, H. W.; Russell, T. P. Characterization of the Morphology of Solution-Processed Bulk Heterojunction Organic Photovoltaics. *Prog. Polym. Sci.* **2013**, *38*, 1990−2052.

(17) Huang, Y.; Kramer, E. J.; Heeger, A. J.; Bazan, G. C. Bulk Heterojunction Solar Cells: Morphology and Performance Relationships. *Chem. Rev.* **2014**, *114*, 7006−7043.

(18) Liang, Y.; Yu, L. A New Class of Semiconducting Polymers for Bulk Heterojunction Solar Cells with Exceptionally High Performance. *Acc. Chem. Res.* **2010**, *43*, 1227−1236.

(19) Ye, L.; Zhang, S.; Huo, L.; Zhang, M.; Hou, J. Molecular Design toward Highly Efficient Photovoltaic Polymers Based on Two-Dimensional Conjugated Benzodithiophene. *Acc. Chem. Res.* **2014**, *47*, 1595−1603.

(20) Li, Y. Molecular Design of Photovoltaic Materials for Polymer Solar Cells: Toward Suitable Electronic Energy Levels and Broad Absorption. *Acc. Chem. Res.* **2012**, *45*, 723−733.

(21) Chen, Y.; Wan, X.; Long, G. High Performance Photovoltaic Applications Using Solution-Processed Small Molecules. *Acc. Chem. Res.* **2013**, *46*, 2645−2655.

(22) Lin, Y.; Li, Y.; Zhan, X. Small Molecule Semiconductors for High-Efficiency Organic Photovoltaics. *Chem. Soc. Rev.* **2012**, *41*, 4245−4272.

(23) Fitzner, R.; Mena-Osteritz, E.; Mishra, A.; Schulz, G.; Reinold, E.; Weil, M.; Körner, C.; Ziehlke, H.; Elschner, C.; Leo, K.; et al. Correlation of π-Conjugated Oligomer Structure with Film Morphology and Organic Solar Cell Performance. *J. Am. Chem. Soc.* **2012**, *134*, 11064−11067.

(24) Ma, W.; Yang, C.; Gong, X.; Lee, K.; Heeger, A. J. Thermally Stable, Efficient Polymer Solar Cells with Nanoscale Control of the Interpenetrating Network Morphology. *Adv. Funct. Mater.* **2005**, *15*, 1617−1622.

(25) Peet, J.; Kim, J. Y.; Coates, N. E.; Ma, W. L.; Moses, D.; Heeger, A. J.; Bazan, G. C. Efficiency Enhancement in Low-Bandgap Polymer Solar Cells by Processing with Alkane Dithiols. *Nat. Mater.* **2007**, *6*, 497−500.

(26) Kouijzer, S.; Michels, J. J.; van den Berg, M.; Gevaerts, V. S.; Turbiez, M.; Wienk, M. M.; Janssen, R. A. J. Predicting Morphologies of Solution Processed Polymer:Fullerene Blends. *J. Am. Chem. Soc.* **2013**, *135*, 12057−12067.

(27) Wei, G.; Wang, S.; Sun, K.; Thompson, M. E.; Forrest, S. R. Solvent-Annealed Crystalline Squaraine: $PC_{70}BM$ (1:6) Solar Cells. *Adv. Energy Mater.* **2011**, *1*, 184−187.

(28) Zhang, J.; Zhang, Y.; Fang, J.; Lu, K.; Wang, Z.; Ma, W.; Wei, Z. Conjugated Polymer-Small Molecule Alloy Leads to High Efficient Ternary Organic Solar Cells. *J. Am. Chem. Soc.* **2015**, *137*, 8176−8183.

(29) Fu, Y. T.; da Silva Filho, D. A.; Sini, G.; Asiri, A. M.; Aziz, S. G.; Risko, C.; Brédas, J. L. Structure and Disorder in Squaraine:C_{60} Organic Solar Cells: A Theoretical Description of Molecular Packing and Electronic Coupling at the Donor:Acceptor Interface. *Adv. Funct. Mater.* **2014**, *24*, 3790−3798.

(30) Wang, T.; Ravva, M. K.; Brédas, J. L. Impact of the Nature of the Side-Chains on the Polymer-Fullerene Packing in the Mixed Regions of Bulk Heterojunction Solar Cells. *Adv. Funct. Mater.* **2016**, *26*, 5913−5921.

(31) Jackson, N. E.; Kohlstedt, K. L.; Savoie, B. M.; Olvera de la Cruz, M.; Schatz, G. C.; Chen, L. X.; Ratner, M. A. Conformational Order in Aggregates of Conjugated Polymers. *J. Am. Chem. Soc.* **2015**, *137*, 6254−6262.

(32) D'Avino, G.; Muccioli, L.; Zannoni, C. From Chiral Islands to Smectic Layers: A Computational Journey Across Sexithiophene Morphologies on C_{60}. *Adv. Funct. Mater.* **2015**, *25*, 1985−1995.

(33) Han, G.; Shen, X.; Duan, R.; Geng, H.; Yi, Y. Revealing the Influence of the Solvent Evaporation Rate and Thermal Annealing on the Molecular Packing and Charge Transport of $DPP(TBFu)_2$. *J. Mater. Chem. C* **2016**, *4*, 4654−4661.

(34) Reddy, S. Y.; Kuppa, V. K. Molecular Dynamics Simulations of Organic Photovoltaic Materials: Structure and Dynamics of Oligothiophene. *J. Phys. Chem. C* **2012**, *116*, 14873−14882.

(35) Long, G.; Li, A.; Shi, R.; Zhou, Y. C.; Yang, X.; Zuo, Y.; Wu, W. R.; Jeng, U. S.; et al. The Evidence for Fullerene Aggregation in High-Performance Small-Molecule Solar Cells by Molecular Dynamics Simulation. *Adv. Electron. Mater.* **2015**, *1*, 1500217.

(36) Groves, C.; Greenham, N. Monte Carlo Simulations of Organic Photovoltaics. *Top. Curr. Chem.* **2013**, *352*, 257−278.

(37) Watkins, P. K.; Walker, A. B.; Verschoor, G. L. B. Dynamical Monte Carlo Modelling of Organic Solar Cells: The Dependence of Internal Quantum Efficiency on Morphology. *Nano Lett.* **2005**, *5*, 1814−1818.

(38) Gemünden, P.; Poelking, C.; Kremer, K.; Andrienko, D.; Daoulas, K. C. Nematic Ordering, Conjugation, and Density of States of Soluble Polymeric Semiconductors. *Macromolecules* **2013**, *46*, 5762−5774.

(39) Alexiadis, O.; Mavrantzas, V. G. All-Atom Molecular Dynamics Simulation of Temperature Effects on the Structural, Thermodynamic,

DOI: 10.1021/acs.jpcc.6b11824
J. Phys. Chem. C 2017, 121, 5864−5870

and Packing Properties of the Pure Amorphous and Pure Crystalline Phases of Regioregular P3HT. *Macromolecules* **2013**, *46*, 2450−2467.
(40) Cheung, D. L.; Troisi, A. Theoretical Study of the Organic Photovoltaic Electron Acceptor PCBM: Morphology, Electronic Structure, and Charge Localization. *J. Phys. Chem. C* **2010**, *114*, 20479−20488.
(41) Qin, T.; Troisi, A. Relation between Structure and Electronic Properties of Amorphous MEH-PPV Polymers. *J. Am. Chem. Soc.* **2013**, *135*, 11247−11256.
(42) Steiner, F.; Foster, S.; Losquin, A.; Labram, J.; Anthopoulos, T. D.; Frost, J. M.; Nelson, J. Distinguishing the Influence of Structural and Energetic Disorder on Electron Transport in Fullerene Multi-Adducts. *Mater. Horiz.* **2015**, *2*, 113−119.
(43) To, T. T.; Adams, S. Modelling of P3HT:PCBM Interface using Coarse-Grained Forcefield Derived from Accurate Atomistic Force Field. *Phys. Chem. Chem. Phys.* **2014**, *16*, 4653−4663.
(44) Carrillo, J. M.; Kumar, R.; Goswami, M.; Sumpter, B. G.; Brown, W. M. New Insights into the Dynamics and Morphology of P3HT:PCBM Active Layers in Bulk Heterojunctions. *Phys. Chem. Chem. Phys.* **2013**, *15*, 17873−17882.
(45) Lee, C. K.; Pao, C. W.; Chu, C. W. Multiscale Molecular Simulations of the Nanoscale Morphologies of P3HT:PCBM Blends for Bulk Heterojunction Organic Photovoltaic Cells. *Energy Environ. Sci.* **2011**, *4*, 4124−4132.
(46) Xu, X.; Ji, Y.; Du, C.; Hou, T.; Li, Y. The Prediction of the Morphology and PCE of Small Molecular Organic Solar Cells. *RSC Adv.* **2015**, *5*, 70939−70948.
(47) Jankowski, E.; Marsh, H. S.; Jayaraman, A. Computationally Linking Molecular Features of Conjugated Polymers and Fullerene Derivatives to Bulk Heterojunction Morphology. *Macromolecules* **2013**, *46*, 5775−5785.
(48) Lee, C. K.; Hua, C. C.; Chen, S. A. Phase Transition and Gels in Conjugated Polymer Solutions. *Macromolecules* **2013**, *46*, 1932−1938.
(49) Huang, D. M.; Faller, R.; Do, K.; Moulé, A. J. Coarse-Grained Computer Simulations of Polymer/Fullerene Bulk Heterojunctions for Organic Photovoltaic Applications. *J. Chem. Theory Comput.* **2010**, *6*, 526−537.
(50) Zhang, Q.; Kan, B.; Liu, F.; Long, G.; Wan, X.; Chen, X.; Zuo, Y.; Ni, W.; Zhang, H.; Li, M.; et al. Small-Molecule-Based Solar Cells with Efficiency Over 9%. *Nat. Photonics* **2015**, *9*, 35−41.
(51) Wang, Y.; Izvekov, S.; Yan, T.; Voth, G. A. Multiscale Coarse-Graining of Ionic Liquids. *J. Phys. Chem. B* **2006**, *110*, 3564−3575.
(52) Noid, W.; Liu, P.; Wang, Y.; Chu, J. W.; Ayton, G. S.; Izvekov, S.; Andersen, H. C.; Voth, G. A. The Multiscale Coarse-Graining Method. II. Numerical Implementation for Coarse-Grained Molecular Models. *J. Chem. Phys.* **2008**, *128*, 244115.
(53) Forester, T. R.; Smith, W. *Dl_Poly User Manual*; CCLRC, Daresbury Laboratory: Daresbury, Warrington, U.K., 1995.
(54) Frisch, M. J.; Trucks, G. W.; Schlegel, H. B.; Scuseria, G. E.; Robb, M. A.; Cheeseman, J. R.; Scalmani, G.; Barone, V.; Mennucci, B.; Petersson, G. A.; et al. *Gaussian 09*, Revision B.01; Gaussian, Inc.: Wallingford, CT, 2010.
(55) Wang, Y.; Voth, G. A. Tail Aggregation and Domain Diffusion in Ionic Liquids. *J. Phys. Chem. B* **2006**, *110*, 18601−18608.
(56) Wang, Y.; Feng, S.; Voth, G. A. Transferable Coarse-Grained Models for Ionic Liquids. *J. Chem. Theory Comput.* **2009**, *5*, 1091−1098.
(57) Sun, K.; Xiao, Z.; Lu, S.; Zajaczkowski, W.; Pisula, W.; Hanssen, E.; White, J. M.; Williamson, R. M.; Subbiah, J.; Ouyang, J.; et al. A Molecular Nematic Liquid Crystalline Material for High-Performance Organic Photovoltaics. *Nat. Commun.* **2015**, *6*, 6013−6021.
(58) Chandler, D. Interfaces and the Driving Force of Hydrophobic Assembly. *Nature* **2005**, *437*, 640−647.
(59) Wu, W. R.; Jeng, U. S.; Su, C. J.; Wei, K. H.; Su, M. S.; Chiu, M. Y.; Chen, C. Y.; Su, W. B.; Su, C. H.; Su, A. C. Competition between Fullerene Aggregation and Poly(3-hexylthiophene) Crystallization upon Annealing of Bulk Heterojunction Solar Cells. *ACS Nano* **2011**, *5*, 6233−6243.
(60) Long, G.; Wu, B.; Solanki, A.; Yang, X.; Kan, B.; Liu, X.; Wu, D.; Xu, Z.; Wu, W. R.; Jeng, U. S.; et al. New Insights into the Correlation between Morphology, Excited State Dynamics, and Device Performance of Small Molecule Organic Solar Cells. *Adv. Energy Mater.* **2016**, *6*, 1600961.

DOI: 10.1021/acs.jpcc.6b11824
J. Phys. Chem. C 2017, 121, 5864−5870